ACS APPLIED MATERIALS & INTERFACES

Research Article

www.acsami.org

Surface Molecular Tailoring Using pH-Switchable Supramolecular Dendron-Ligand Assemblies

Parvez Iqbal,[†] Frankie J. Rawson,[‡] Watson K.-W. Ho,[§] Siu-Fung Lee,[§] Ken Cham-Fai Leung,[§,#] Xingyong Wang,[∥] Akash Beri,[†,⊥] Jon A. Preece,[⊥] Jing Ma,[∥] and Paula M. Mendes*[,†]

[†]School of Chemical Engineering and [⊥]School of Chemistry, University of Birmingham, Birmingham B15 2TT, United Kingdom

[‡]Laboratory of Biophysics and Surface Analysis, School of Pharmacy, University of Nottingham, University Park, Nottingham NG72RD, United Kingdom

[§]Department of Chemistry, The Chinese University of Hong Kong, Shatin NT, Hong Kong SAR

[#]Department of Chemistry and Institute of Creativity and Institute of Molecular Functional Materials, University Grants Committee, The Hong Kong Baptist University, Kowloon Tong, Kowloon, Hong Kong SAR

[∥]School of Chemistry and Chemical Engineering, Nanjing University, Nanjing 210093, P. R. China

Supporting Information

ABSTRACT: The rational design of materials with tailored properties is of paramount importance for a wide variety of biological, medical, electronic and optical applications. Here we report molecular level control over the spatial distribution of functional groups on surfaces utilizing self-assembled monolayers (SAMs) of pH-switchable surface-appended pseudorotaxanes. The supramolecular systems were constructed from a poly(aryl ether) dendron-containing a dibenzo[24]crown-8 (DB24C8) macrocycle and a thiol ligand-containing a dibenzylammonium recognition site and a fluorine end group. The dendron establishes the space (dendritic effect) that each pseudorotaxane occupies on the SAM. Following SAM formation, the dendron is released from the surface by switching off the noncovalent interactions upon pH stimulation, generating surface materials with tailored physical and chemical properties.

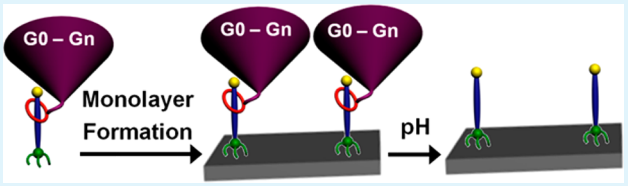

KEYWORDS: *self-assembly, binary self-assembled monolayers, functional surfaces, supramolecular systems, pseudorotaxanes*

INTRODUCTION

The development of self-assembly processes capable of generating functional surfaces with well-defined and tunable properties promises to have far-reaching consequences for biological and medical applications.[1−4] Furthermore, these self-assembly processes can lead to the preparation and tailoring of intricate surfaces with unique properties for electronic and optical applications.[5] The ability of molecular compounds to self-assemble on surfaces, giving rise to self-assembled monolayers (SAMs),[6,7] has been exploited extensively over the past decade to modify and tailor the properties of a wide range of metal, metal oxides and semiconductor surfaces. Recently, mixed SAMs have been the subject of much interest from the viewpoint of tailoring the spacing of chemical functional groups on the surface, and ultimately controlling the surface wettability, friction, and adhesion properties of surfaces and the density of biomolecules in biochips, biosensors, and medical electronic devices.[8−14]

Mixed SAMs rely on preparing SAMs from a solution of two or more molecular compounds, which usually have different end group functionalities. This process has several limitations such as the fact that the ratio of the two compounds in the monolayer is rarely identical to their ratio in the solution, because of the preferential adsorption of one of the components. This preferential adsorption means control over not only the density but also the homogeneity of functional groups in mixed monolayers is not straightforward.[15] Thus, the formation of two-component monolayers has been reported by several authors[16−18] to lead to phase-segregated heterogeneous mixed SAMs with surface ratios different from solution ratios of the components. If we can assemble molecular components in which functional groups are deterministically arranged with special distributions on the molecular scale, we will open access to a new class of surface materials with designed and tailored physical and chemical properties. Starting from this premise, we have devised pH-switchable supramolecular systems that are able to self-assemble on surfaces and contain a molecular component that can vary in steric bulkiness (Figure 1). Poly(aryl ether) dendrons with generations varying from 0 to n ([G0]−[G_n]) serve as ideal steric molecular components because of their precisely controllable size, molecular weight, and hydrophobic and inert chemical composition.[19] The dendrons act as space-filling molecular moieties that establish the space that each pseudorotaxane occupies on the surface. Furthermore, the dendrons are bound to the surface by noncovalent interactions and can be released after SAM

Received: September 17, 2013
Accepted: April 17, 2014
Published: April 17, 2014

   dx.doi.org/10.1021/am501613c | ACS Appl. Mater. Interfaces 2014, 6, 6264−6274

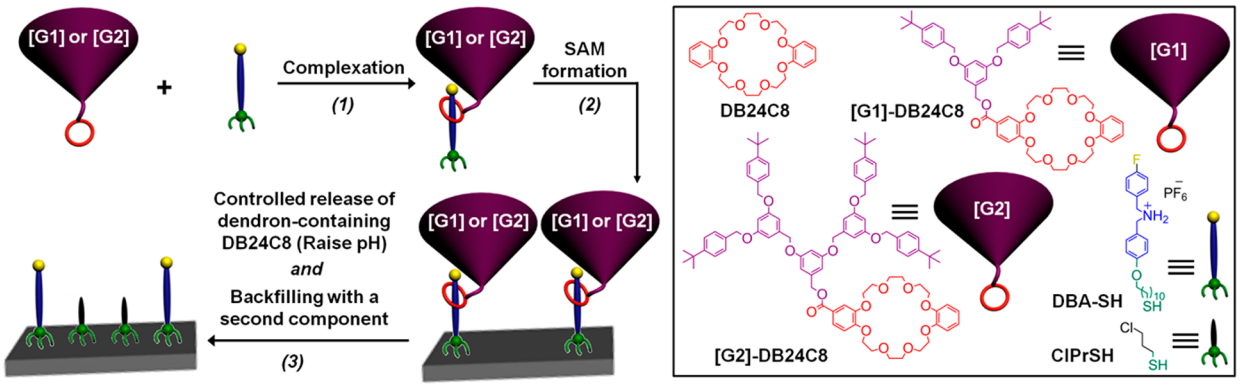

Figure 1. Schematic representation of an effective strategy to control the density and spatial distribution of functional groups on surfaces. The strategy involves three main steps: (1) self-assembly of pH-switchable supramolecular systems comprising a polyaryl dendron-containing dibenzo[24]crown-8 (DB24C8) and a dibenzylammonium (DBA) thread with a fluorine end functional group and a thiol surface-active headgroup; (2) SAM formation of the pH-switchable supramolecular systems on gold surfaces; (3) simultaneous decomplexation of the DB24C8-functionalized dendrons from the SAM on addition of a base and self-assembly of a second component (i.e., ClPrSH) on the vacant space previously occupied by the dendrons.

formation simply by switching off the noncovalent interactions upon raising the pH. Removal of the noncovalently bound dendron spacing groups will expose functional groups on the surface. Thus, by carefully selecting the dendron component, it should be possible to tailor at the molecular level the density and spatial distribution of functional groups on material surfaces.

The supramolecular system is based on host–guest inclusion complex formation between a poly(aryl ether) dendron-containing dibenzo[24]crown-8 (DB24C8) and a dibenzylammonium (DBA) thread with a fluorine end functional group and a thiol surface-active headgroup for strong anchoring onto the gold surface upon SAM formation (Figure 1). The assembly and disassembly processes of the supramolecular system based on DB24C8/DBA pseudorotaxane can be controlled simply by acid–base reactions.[20−24] The DB24C8⊃DBA pseudorotaxane complex is self-assembled and stabilized by [N^+–H···O] and [N^+C–H···O] hydrogen bonds, which are easily destabilized by deprotonation and raising the pH, and re-established by acidifying. Moreover, additional [C–H···O] and π–π stacking interactions, as well as electrostatic forces, also contribute to the stability of the pseudorotaxane's formation. In this study, three supramolecular systems were constructed by the self-assembly of (i) DB24C8 with the DBA thiol derivative (DBA-SH), (ii) [G1] poly(aryl ether) dendron-containing DB24C8 ([G1]-DB24C8) with DBA-SH and (iii) [G2]-DB24C8 with DBA-SH. SAMs of these systems were prepared on gold surfaces, followed by decomplexation and simultaneous backfilling with 3-chloropropanethiol (ClPrSH) to form mixed monolayers (Figure 1). This strategy was investigated for its applicability and effectiveness on providing molecular level control over density and spatial distribution of functional groups in a monolayer.

RESULTS AND DISCUSSION

Synthesis. The DBA-SH, DB24C8, [G1]-DB24C8, and [G2]-DB24C8 were synthesized via multistep synthetic routes. The synthesis of DBA-SH was initiated with the alkylation of 4-hydroxybenzaldehyde by 11-bromoundecene in the presence of K_2CO_3 and NaI to obtain aldehyde **1** (Scheme 1). Fluorobenzylamine was reacted with aldehyde **1** at an elevated temperature to afford the imine, which was subsequently

Scheme 1. Synthesis of DBA-SH; (i) 11-bromoundecene, K_2CO_3, Acetone, Reflux, 16 h, 81%, (ii) 4-Flourobenzylamine, PhMe, Reflux, N_2(g), 20 h, (iii) $NaBH_4$, MeOH, Reflux, N_2(g), 20 h, 85%, (iv) Boc_2O, NEt_3, 4-DMAP (cat), THF, rt, N_2(g), 16 h, 71%, (v) HSAc, AIBN (cat), PhMe, Reflux, 2 h, 84%, (vi) TFA, DCM, rt, N_2(g), 6 h, 80%, (vii) 0.1 M HCl, MeOH, N_2(g), 4 h, 71% %, (viii) HPF_6, DCM, rt, N_2(g), 10 min, 91%

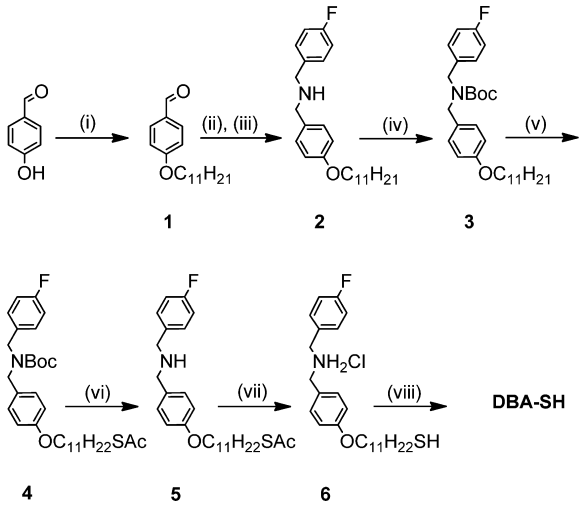

reduced to the secondary amine **2** with $NaBH_4$. Amine-Boc protection was performed via reaction of **2** with Boc_2O in the presence of NEt_3 and catalytic amount of 4-DMAP to obtain **3**. Thioacetylation of **3** was performed via the addition of thioacetic acid to the alkene moiety of **3**, with a catalytic amount of AIBN to afford the thioacetate **4**. Boc deprotection of thiocetate **4** was carried out under acidic conditions (TFA) to yield the secondary amine **5**. The thioacetate moiety in **5** was acid hydrolyzed (0.1 M HCl) to give the thiol **6**, followed by protonation of the secondary amine with HPF_6 to afford the desired DBA-SH as the hexafluorophosphate salt.

[G1]- and [G2]-dendritic alcohols and macrocycle **7** were synthesized according to literature procedures[11,12] (for further details, see the Supporting Information). Macrocycle **7** was base hydrolyzed (NaOH) to afford the desired carboxylic acid functionalized crown ether **8**. [G1]- and [G2]-dendritic

dx.doi.org/10.1021/am501613c | ACS Appl. Mater. Interfaces 2014, 6, 6264−6274

alcohols were DCC coupled to carboxylic acid functionalized crown ether **8** with catalytic amount of DMAP to afford the desired esters [G1]-DB24C8 and [G2]-DB24C8 (Scheme 2).

Scheme 2. Synthesis of Poly(aryl ether) Dendron-Containing DB24C8 (i) NaOH(aq) EtOH, reflux, 16 h, 80%, (ii) DCC, 4-DMAP, DCM, rt, N_2(g), 16 h, 54% ([G1]-DB24C8), 24% ([G2]-DB24C8)

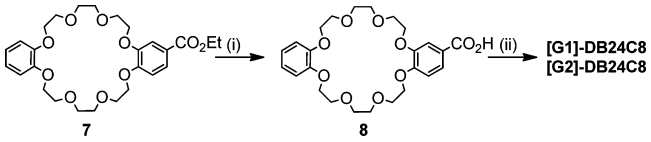

Complexation. The DB24C8⊃DBA-SH, [G1]-DB24C8⊃DBA-SH, and [G2]-DB24C8⊃DBA-SH pseudorotaxanes were formed by complexation of DBA-SH with 2 equiv. of either DB24C8, [G1]-DB24C8 or [G2]-DB24C8 in HPLC MeCN and confirmed by ^{1}H NMR spectroscopy (MeCN-d_3, 300 MHz, 25 °C). By way of an example, Figure 2 shows the

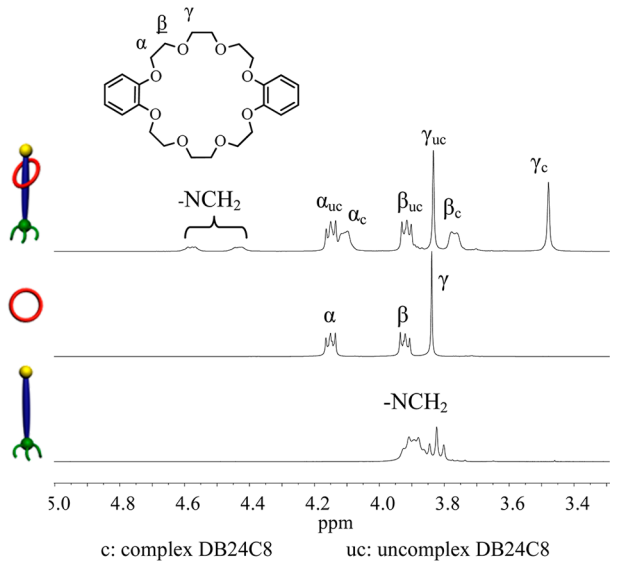

Figure 2. Partial ^{1}H NMR (300 MHz, MeCN-d_3, 25 °C, 10 mM) spectra of DBA-SH, DB24C8, and DB24C8⊃DBA-SH.

partial ^{1}H NMR spectra of DB24C8, DBA-SH and DB24C8⊃DBA-SH. The characteristic ^{1}H NMR peaks corresponding to the α, β, γ protons on the crown ether are shifted upfield from 4.10, 3.82, and 3.70 ppm to 3.96, 3.50, and 3.40 ppm, respectively, after the addition of DBA-SH, whereas the benzylic methylene protons are shifted downfield from 3.80 to 3.90 ppm to 4.40−4.50 ppm. These are common shifts observed when complexation between crown ether and DBA takes place.[9,13] By integrating the complexed and uncomplexed ^{1}H NMR resonances belonging to the α, β, γ protons on the crown ether, it was determined that >95% of DBA-SH complexed to DB24C8. Comparable values of complexation above 95% were obtained between DBA-SH and either [G1]-DB24C8 or [G2]-DB24C8.

SAM Preparation and Characterization. SAMs of the DB24C8⊃DBA-SH, [G1]-DB24C8⊃DBA-SH, and [G2]-DB24C8⊃DBA-SH supramolecular assemblies were formed by immersing freshly plasma cleaned Au substrates in 10 mM MeCN solutions of the supramolecular complexes for 24 h. In order to create the mixed SAMs, the freshly prepared SAMs of pH-switchable supramolecular dendron-thiol ligand systems were immersed in a mixed MeCN solution of 2 mM NEt_3 and 1 mM ClPrSH for 30 min. It is important to note that the backfilling conditions with ClPrSH have been previously demonstrated by us[12] not to affect the spatial distribution of a previously immobilized thiol. Pure DBA-SH and ClPrSH SAMs, which were used as controls, were prepared in MeCN solutions of 10 mM DBA-SH and 1 mM ClPrSH, respectively, for 24 h.

SAM formation was evaluated by ellipsometry, contact angle (Table 1) and XPS (Figure 3 and Table 2). The advancing contact angle (θ_{adv}) observed for pure monolayer of DBA-SH is 101 ± 1°, which is in good agreement with the literature for fluorine-terminated monolayers (Table 1).[25] Note that the hysteresis ($\theta_{adv} - \theta_{rec}$) value of 33° suggests the presence of a sparsely packed monolayer, which is likely due to the electrostatic repulsions of the protonated amino group in DBA-SH. The θ_{adv} of 83 ± 1° for ClPrSH SAM is consistent with previous reports on chlorine-terminated SAMs,[26] where the hysteresis of 34° indicates once more the presence of a loosely packed SAM. The lack of order in this monolayer is most likely a result of the weak interactions between the short alkyl chains of the ClPrSH SAM.[27]

The wettability properties of the monolayers formed from the DB24C8⊃DBA-SH, [G1]-DB24C8⊃DBA-SH, and [G2]-DB24C8⊃DBA-SH supramolecular assemblies are lower than for pure DBA-SH monolayer, with observed θ_{adv} of 95 ± 3, 91 ± 2, and 87 ± 2°, respectively. It is assumed that this decrease in wettability is due to the concealment of the very hydrophobic fluorine end group by the longer DBA-SH

Table 1. Advancing (θ_a) and Receding (θ_r) Water Contact Angles and Ellipsometric Thickness for the SAMs Formed

SAM		contact angle (deg)		thickness (nm)	
		θ_a	θ_r	ellipsometric	theoretical[b]
DBA-SH		101 ± 1	68 ± 1	2.00 ± 0.08	2.40
ClPrSH		83 ± 1	49 ± 3	0.42 ± 0.01	0.51
DB24C8⊃DBA-SH	complexed	95 ± 3	44 ± 4	1.85 ± 0.10	2.27
	mixed[a]	92 ± 1	57 ± 2	1.78 ± 0.08	
[G1]-DB24C8⊃DBA-SH	complexed	91 ± 4	42 ± 3	1.70 ± 0.07	2.11
	mixed[a]	89 ± 1	56 ± 3	1.65 ± 0.08	-
[G2]-DB24C8⊃DBA-SH	complexed	89 ± 3	43 ± 2	1.60 ± 0.05	1.69
	mixed[a]	87 ± 2	55 ± 2	1.45 ± 0.05	

[a]DBA-SH:ClPrSH mixed SAM that was prepared by the initial formation of a supramolecular complex monolayer, followed by simultaneous decomplexation and immersion in a ClPrSH solution. [b]Calculated via MD simulations.

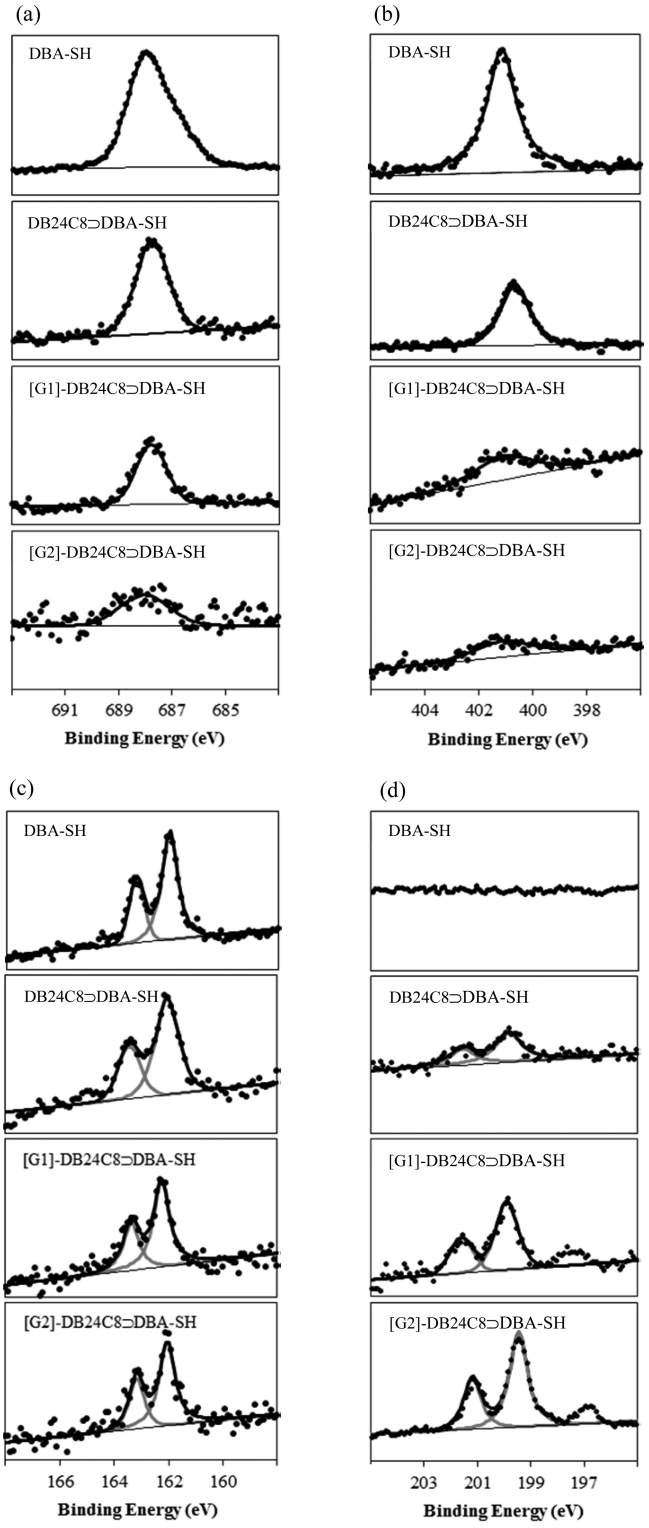

Figure 3. XPS spectra of (a) F (1s), (b) N (1s), (c) S (2p), and (d) Cl (2p) for pure DBA-SH and mixed monolayers formed from DB24C8⊃DBA-SH, [G1]-DB24C8⊃DBA-SH, and [G2]-DB24C8⊃DBA-SH.

molecule and the terminal end groups belonging to the crown ether or dendrons. The bulkiness of the supramolecular assemblies, which are expected to induce steric effects and complex intermolecular interactions during the self-assembly process, is most likely responsible for the higher contact angle hysteresis observed when compared with the pure DBA-SH SAM.

After decomplexation of DB24C8⊃DBA-SH, [G1]-DB24C8⊃DBA-SH, and [G2]-DB24C8⊃DBA-SH monolayers by means of a base and simultaneous immersion in a ClPrSH solution, the resulting mixed monolayers exhibit θ_{adv} of 92 ± 3, 89 ± 2, and 87 ± 2°, respectively. The θ_{adv} values obtained are between those of pure DBA-SH (101 ± 1°) and ClPrSH (83 ± 1°) SAMs, and thus consistent with the presence of a DBA-SH:ClPrSH mixed monolayer. Interestingly, the contact angle hysteresis obtained for the mixed monolayers are between 12 and 14° lower than the respective complexed monolayers and comparable to the pure DBA-SH and ClPrSH SAMs. Using the θ_{adv} measurements of the pure and DBA-SH:ClPrSH mixed monolayers in conjunction with the application of the Cassie's equation,[28] the ratio of the two surfactants (DBA-SH and ClPrSH) on the mixed monolayers was determined. Cassie's eq 1 relates the contact angle of a surface of mixed composition to those of pure SAMs

$$\cos \theta_{adv} = x\cos \theta_{adv1} + y\cos \theta_{adv2} \quad (1)$$

Where θ_{adv} is the water advancing contact angle on the mixed SAM, θ_{adv1} and θ_{adv2} are the contact angles related to the pure SAMs, in this case, formed from DBA-SH and ClPrSH, respectively. x and y are the corresponding surface molar ratios of DBA-SH and ClPrSH, with $x + y = 1$. By employing this relationship between surface wettability and the surface composition of the mixed SAMs, molar ratios (DBA-SH:ClPrSH) in the mixed SAMs of 1:1, 1:2, and 1:3 were obtained depending on if they were initially formed from either DB24C8⊃DBA-SH, [G1]-DB24C8⊃DBA-SH, or [G2]-DB24C8⊃DBA-SH monolayers, respectively. A trend is shown that indicates that the molar ratio between DBA-SH and ClPrSH decreases as the steric bulk of the initial supramolecular complex increases.

The ellipsometric thickness observed for the different monolayers is shown in Table 1. The monolayer thicknesses obtained for pure DBA-SH and ClPrSH are 2.00 ± 0.08 nm and 0.42 ± 0.01 nm, respectively. These values are in good agreement with the theoretical thicknesses of 2.40 and 0.51 nm, which were calculated through molecular dynamics (MD) simulations for DBA-SH and ClPrSH SAMs on gold surface, respectively (see the Supporting Information for simulation details).

The SAMs of the supramolecular complexes and subsequent mixed monolayers exhibit lower thickness values when compared to pure DBA-SH SAM. Once more, a trend is observed showing that with increasing the bulk of the supramolecular assembly, the thickness values of the SAM of the supramolecular complex monolayer diminish. The thicknesses obtained from the MD simulations show the same trend (Table 1), with the snapshots illustrating that the bulky dendrons drag the DBA-SH down to the surface and occupy a larger surface area in the monolayer (Figure S2). Thus, the ellipsometric thickness decrease can be rationalized by considering that the increased size of the supramolecular assembly leads to the occupation of a larger surface area per molecule, which in turn induces a decrease in the SAM density. Consequently, the reduced monolayer densification is reflected in lower ellipsometric thickness values. Another trend that can be observed is that the thickness of the DBA-SH:ClPrSH mixed monolayer decreases with the steric bulkiness of the initial supramolecular complex. These results can be regarded as a

Table 2. Elemental Ratios in the SAMs Formed from Complexed Molecules (complexed) and after Immersion in Mixed Solution of NEt_3 and ClPrSH (mixed) Obtained via the XPS Data

	DB24C8⊃DBA-SH		[G1]-DB24C8⊃DBA-SH		[G2]-DB24C8⊃DBA-SH	
XPS ratio	complexed	mixed	complexed	mixed	complexed	mixed
Au/N	18.87 ± 4.64	16.67 ± 6.67	33.30 ± 7.77	33.56 ± 8.79	47.03 ± 7.93	46.34 ± 8.09
S/F	1.05 ± 0.05	2.00 ± 0.10	1.06 ± 0.10	3.09 ± 0.19	1.10 ± 0.06	4.18 ± 0.15
S/N	1.07 ± 0.07	2.03 ± 0.11	1.04 ± 0.11	3.06 ± 0.12	1.03 ± 0.05	4.12 ± 0.25
S/Cl		2.05 ± 0.13		1.52 ± 0.12		1.25 ± 0.20
Cl/F		0.98 ± 0.08		2.03 ± 0.19		3.34 ± 0.21
Cl/N		0.99 ± 0.09		2.01 ± 0.12		3.30 ± 0.18

demonstration of an increased amount of the shortest chain, i.e., ClPrSH, in the DBA-SH:ClPrSH mixed SAM by using supramolecular complexes with increasing bulk.

To investigate whether the presence of excess DB24C8, [G1]-DB24C8, or [G2]-DB24C8 influenced the experimental obtained monolayer thicknesses, freshly plasma-cleaned Au substrates were immersed for 24 h in 20 mM HPLC MeCN solutions of the three molecules. The ellipsometric thicknesses of the DB24C8, [G1]-DB24C8, or [G2]-DB24C8 immersed substrates were determined to be 0.20 ± 0.03 nm, 0.18 ± 0.05 nm, and 0.19 ± 0.04 nm. These thicknesses are similar to those found in freshly cleaned Au substrate (0.25 ± 0.06 nm), suggesting that the DB24C8, [G1]-DB24C8, or [G2]-DB24C8 interact weakly with the gold surface and are readily removed through rinsing with copious amounts of HPLC MeCN.

XPS further confirms the formation of the pure DBA-SH, pure ClPrSH, and complexed and mixed monolayers, showing signals from F (1s), N (1s), and S (2p) on all surfaces (Figure 3). The spectra display N (1s) peaks at 401.4 eV and F (1s) peaks at 688 eV. No peaks are observed in the P (2p) region in the pure DBA-SH and complexed (DB24C8⊃DBA-SH, [G1]-DB24C8⊃DBA-SH, or [G2]-DB24C8⊃DBA-SH) monolayers, hence suggesting that the counteranion PF_6^- is not present on the SAM surface. Thus, the F (1s) peaks observed correspond to the fluorine end group on the DBA-SH molecule. The S (2p) spectra for all the surfaces show doublet peaks at 163.4 eV (S ($2p_{1/2}$)) and 162.2 eV (S ($2p_{3/2}$)), which are assignable to the thiolate-type sulfur bound to the gold surface.[29]

The presence of the ClPrSH molecule in the mixed monolayers was demonstrated by the appearance of an additional doublet peak between 202 and 199 eV, which corresponds to Cl (2p) (Figure 3d).[30] The Cl ($2p_{1/2}$) and Cl ($2p_{3/2}$) double peak is observed at 201.4 and 199.8 eV, respectively, indicative of a chlorine bound to carbon.[31] In contrast with a decrease in the intensity of the fluorine (Figure 3a) and nitrogen peaks (Figure 3b), the chorine peak (Figure 3d) increases with the increased size of the supramolecular assembly. In agreement with contact angle and ellipsometry analysis, these results reflect the presence of a lower ratio of DBA-SH:ClPrSH in the mixed monolayers as the steric bulk of the initial supramolecular complex increases.

XPS was further used to determine the composition (DBA-SH and ClPrSH) of the mixed monolayers. By integrating the areas of the F (1s), N (1s), S (2p), and Cl (2p) peaks, we were able to calculate the ratios of the various elements (e.g., S/Cl, Cl/F, and Cl/N) on the complexed and mixed monolayers as shown in Table 2. For each monolayer, three independent samples were analyzed by XPS. The samples were found to be reproducible with a moderately low variability. For the mixed monolayers formed from DB24C8⊃DBA-SH, the S/Cl ratio was determined as 2.05 ± 0.13 (i.e., a S:Cl ratio of 2:1). In the same manner, Cl/F and Cl/N ratios were determined to be 0.98 ± 0.08 (i.e., a Cl:F ratio of 1:1) and 0.99 ± 0.09 (i.e., a Cl:N ratio of 1:1), respectively. Because the ClPrSH consists of 1 Cl atom and 1 S atom, and the DBA-SH comprises 1 F atom, 1 N atom and 1 S atom, the ratios above indicate that the mixed monolayers formed from DB24C8⊃DBA-SH are composed of 1:1 ratio of DBA-SH and ClPrSH. Similar XPS analysis were performed on the mixed monolayers formed from the [G1]-DB24C8⊃DBA-SH complex, and S/Cl, Cl/F and Cl/N ratios of 1.52 ± 0.12, 2.03 ± 0.19, and 2.01 ± 0.12, respectively, were obtained. These results reveal the presence of mixed monolayers of DBA-SH and ClPrSH in a 1:2 ratio. Finally, in the mixed monolayers formed from [G2]-DB24C8⊃DBA-SH complex, the S/Cl, Cl/F, and Cl/N ratios are shown to be 1.25 ± 0.20, 3.34 ± 0.21, and 3.30 ± 0.18, respectively. These findings are indicative of a 1:3 ratio of the DBA-SH and ClPrSH in the mixed monolayer.

The ratios of the mixed monolayers obtained by XPS are in excellent agreement with the ones derived from contact angle measurements and interpreted by the Cassie equation. It is also important to note that the XPS provides evidence of the formation of homogeneous mixed monolayers. By comparing the Au/N and Au/F ratios of the complexed monolayers with those of the mixed monolayer, the results show the presence of similar ratios, implying that no desorption of the DBA-SH occurs upon decomplexation and backfilling with ClPrSH. To further understand the trends we are seeing in the relationship between the size of the supramolecular assembly and the ratio of the DBA-SH:ClPrSH mixed SAM, the volumes of DB24C8, [G1]-DB24C8 and [G2]-DB24C8 were investigated (Table 3 and Figure 4). It can be seen that the ratio of the volumes (1:2.0:3.2) correlates well with the corresponding ratio of the DBA-SH and ClPrSH in the mixed monolayer. Our results imply that the surface ratio of two components in mixed SAMs can be well-controlled via careful design of the initial supramolecular complex.

Table 3. Volumes Calculated from vdW Surfaces

	DB24C8	[G1]-DB24C8	[G2]-DB24C8
V (nm^3)	0.44	0.88	1.41
V/V_{DB24C8}	1	2.0	3.2

To demonstrate the absence of lateral diffusion of the DBA-SH molecules upon backfilling with ClPrSH on the gold surface and consequent formation of nanoscale phase separated domains, we studied the nanometer-scale mixing characteristics of the formed binary monolayers by voltammetry as previously reported[17] using the reductive desorption of the adsorbed thiol molecules. Linear sweep voltammetry was performed with gold on mica as working electrodes that had SAMs formed on them

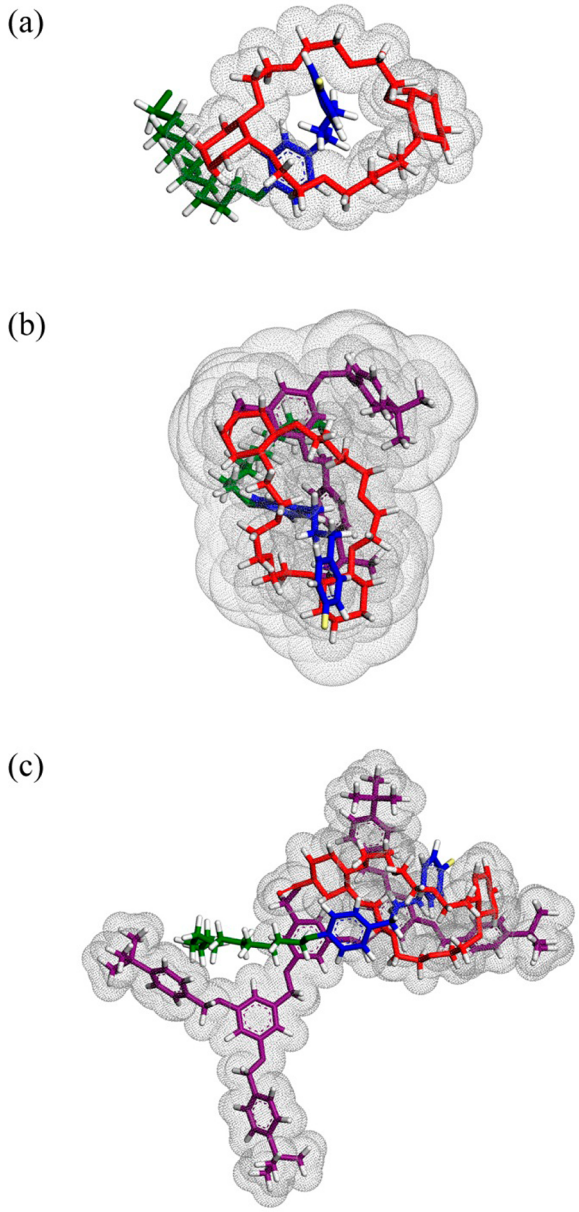

Figure 4. vdW surfaces for (a) DB24C8, (b) [G1]-DB24C8, and (c) [G2]-DB24C8, respectively.

with various constituents, including ClPrSH only, DBA-SH only, DB24C8⊃DBA-SH and DB24C8⊃DBA-SH backfilled with ClPrSH, [G1]-DB24C8⊃DBA-SH only, and [G1]-DB24C8⊃DBA-SH backfilled with ClPrSH, [G2]-DB24C8⊃DBA-SH only, and [G2]-DB24C8⊃DBA-SH backfilled with ClPrSH.

Linear sweep voltammograms were logged with single-component monolayers of ClPrSH and DBA-SH (Figure 5a). Two single peaks were observed at −0.721 V (±0.0028 V) and −1.085 V (±0.007 V) and correspond to the reductive desorption of the adsorbed ClPrSH and DBA-SH, respectively. The difference in the reductive desorption potentials for pure ClPrSH SAMs and pure DBA-SH SAMs is ascribed to the difference in the Gibbs energy of adsorption of the thiols.[17] Because the absence of two distinct reductive peaks in the DBA-SH:ClPrSH SAM indicates the nonexistence of nanoscale phase-separated domains,[17,32] we investigated the reductive desorption of DBA-SH:ClPrSH mixed monolayers formed from DB24C8⊃DBA-SH (Figure 5b), [G1]-DB24C8⊃DBA-SH (Figure 5c), and [G2]-DB24C8⊃DBA-SH (Figure 5d). For comparison purposes, the voltammograms of the complexed monolayers (i.e., DB24C8⊃DBA-SH, [G1]-DB24C8⊃DBA-SH and [G2]-DB24C8⊃DBA-SH) are also plotted in Figure 5b−d, respectively.

For SAMs formed with DB24C8⊃DBA-SH and those backfilled with ClPrSH (Figure 5b), single cathodic peaks were observed at approximately −1.158 ± 0.004 V and −1.146 ± 0.011 V, respectively. Because, following backfilling, the desorption of the DBA-SH:ClPrSH mixed monolayers still displayed a single peak, the results are consistent with the formation of a homogeneous mixed SAM. The formation of DBA-SH:ClPrSH mixed monolayers from [G1]-DB24C8⊃DBA-SH (Figure 5c) and [G2]-DB24C8⊃DBA-SH (Figure 5d) also did not induce phase separation domains, as revealed by the presence of single cathodic peaks for both mixed SAMs. We observed single cathodic peaks at −1.12 ± 0.034 V and −1.11 ± 0.014 V for SAMs formed of [G1]-DB24C8⊃DBA-SH and those backfilled with ClPrSH, respectively, whereas the SAMs formed of [G2]-DB24C8⊃DBA-SH and those backfilled with ClPrSH exhibited single cathodic peaks at −1.128 ± 0.005 V and −1.150 ± 0.041 V, respectively. When a comparison is made between the voltammograms of the different complexed and mixed SAMs and those of pure ClPrSH and DBA-SH, the charge under the desorption peak for the pure SAMs is significantly lower than that of the complexed and mixed SAMs. The desorption charge consists of charge contributions from both faradic processes and capacitance,[33] in which the latter increases for lower packing density in the SAM.[32,34] The lower charge being passed for pure SAMs can thus be explained by the fact that one-component SAMs (i.e., pure ClPrSH and pure DBA-SH SAMs) allow better packing of the SAM, leading to a smaller contribution of the charging current to the total desorption charge. In summary, the fact that we see one single peak for all the mixed SAMs, with no reductive peak observed at the lower potentials associated with pure ClPrSH, confirms that we have a well-mixed binary monolayer without domains and phase separation.[17,32]

It is important to highlight that the absence of diffusion, and thus formation of domains, has been ensured by carrying out the backfilling only for 30 min at room temperature while the dendron has been removed. The simultaneous removal of the dendron and backfilling inhibits any desorption or reorganization of DBA-SH molecule. The results are supported by XPS data, which showed no desorption of the DBA-SH molecule and thus, no exchange takes place with ClPrSH. Furthermore, as previous reported by several groups,[35−37] surface diffusion of thiols at room temperature is extremely slow, with only a raise in temperature increasing such diffusion. The estimated diffusion coefficients are generally reported around 1×10^{-17} to 1×10^{-18} cm^2 s^{-1} at elevated temperatures (e.g., 90−100 °C).[38] Furthermore, studies carry out by Lahann and co-workers[39] also support our results because they have shown that low-density SAMs are structurally stable for 4 weeks under a variety of storage conditions:air at room temperature, argon at room temperature and 4 °C, and ethanol at room temperature. Thus, the linear sweep voltammetry studies and previous literature provide supporting evidence for the absence of lateral diffusion and nanometer-scale phase separation on the gold surfaces.

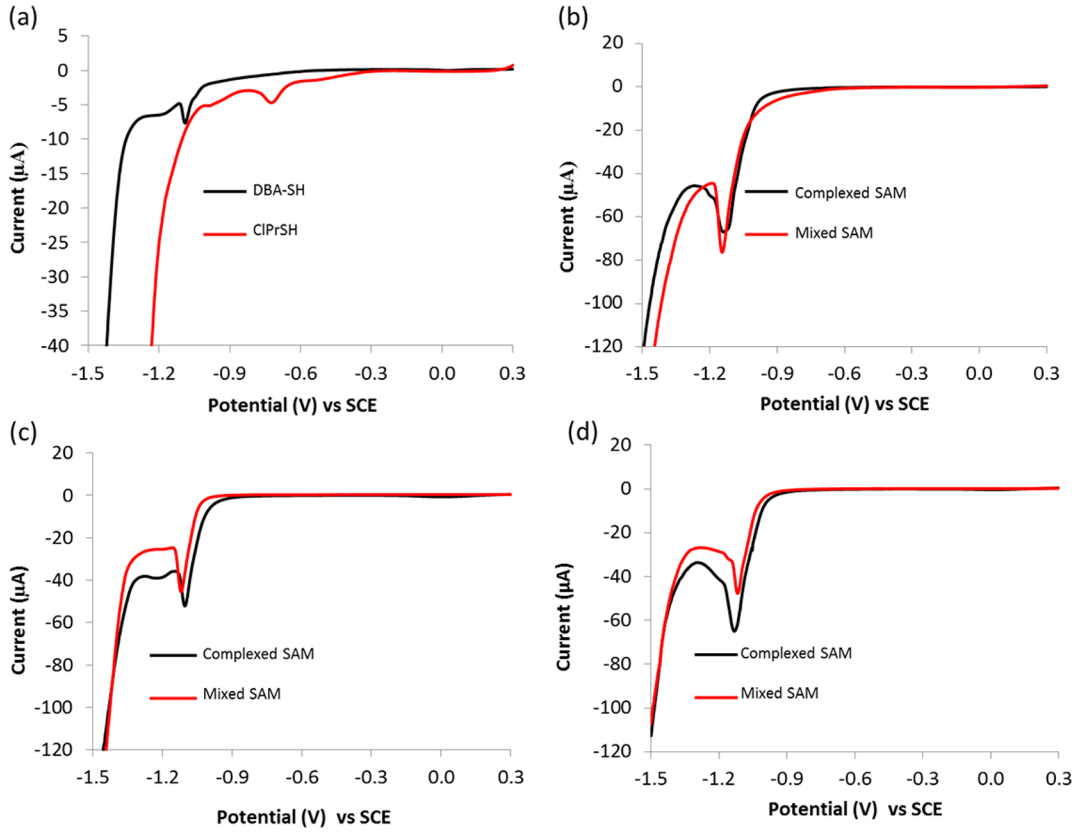

Figure 5. Typical linear sweep voltammograms for reductive thiol desorption obtained for (a) pure DBA-SH and pure ClPrSH SAMs, (b) SAMs formed with DB24C8⊃DBA-SH (i.e., complexed SAMs) and those backfilled with ClPrSH (i.e., mixed SAMs), (c) SAMs formed with [G1]-DB24C8⊃DBA-SH and those backfilled with ClPrSH, and (d) SAMs formed with [G2]-DB24C8⊃DBA-SH and those backfilled with ClPrSH performed at a scan rate of 100 mV s^{-1}.

CONCLUSION

In summary, a powerful and effective methodology for tailoring the spacing of chemical functional groups on material surfaces has been demonstrated through utilizing SAMs of pH-switchable pseudorotaxanes, such as DB24C8⊃DBA-SH, [G1]-DB24C8⊃DBA-SH, or [G2]-DB24C8⊃DBA-SH. Following SAM formation with the supramolecular complexes, the DB24C8-based bulky group is released from the surface by switching off the noncovalent interactions upon pH stimulation, exposing a low-density DBA-SH monolayer on which the vacant space is backfilled with a second functional SAM, i.e., ClPrSH. An incremental increase in the size of the bulky group from DB24C8 to [G1]-DB24C8 and then to [G2]-DB24C8 has led to an incremental decrease in the ratio of the DBA-SH:ClPrSH mixed SAM from 1:1 to 1:2 and then to 1:3, as demonstrated by contact angle and XPS analysis. Molecular dynamics simulations also suggest that the volume of the bulky group increases accordingly. This strategy was elegantly designed, and is sufficiently flexible, to be applied to a broad range of nanoparticles and other nanomaterials. Now that the validity of exploiting supramolecular interactions for the design of surfaces with well-defined density and spatial distribution of functional groups has been established, we anticipate that this strategy will play a significant role in the future of functionalized surface materials for wide variety of biological, medical, electronic, and optical applications.

EXPERIMENTAL SECTION

Materials. Commercially available chemicals were purchased from Sigma-Aldrich and solvents from Fisher Scientific or VWR and used as received. Thin-layer chromatography (TLC) was carried out on aluminum plates coated with silica gel 60 F254 (Merck 5554). For the aryl-based compounds the TLC plates were air-dried and analyzed under a short wave UV lamp (254 nm), whereas for the aliphatic compounds the TLC plates were air-dried and developed in a $KMnO_4$ dip. Column chromatographic separations were performed on silica gel 120 (I24C8 Chrom 32−63, 60 Å).

Synthesis of DBA-SH. *Compound* ***1***. A slurry of 4-hydroxybenzaldehyde (2.09 g, 17.13 mmol), 11-bromoundecene (4.83 g, 20.72 mmol) and K_2CO_3 (4.76 g, 34.49 mmol) in acetone (50 mL) was heated under reflux for 16 h. The resultant reaction mixture was allowed to cool to room temperature and K_2CO_3 was filtered off and the solvent removed in vacuo. The resultant crude solid was dissolved in a minimum amount of DCM and adsorbed onto silica followed by purification by flash column chromatography (gradient elution; 0 to 20% EtOAc in hexane, increase in increments of 10% after each 100 mL of eluent) to yield a white solid (3.83 g, 81%). ^{1}H NMR (300 MHz, $CDCl_3$, Me_4Si, 25 °C) δ_H ppm: 9.86 (s, 1H), 7.81 (d, 2H, J = 8.75 Hz), 6.97 (t, 2H, J = 8.75 Hz), 5.86−5.72 (m, 1H), 5.01−4.89 (m, 2H), 4.01 (t, 2H, J = 6.55 Hz), 2.05−1.98 (m, 2H), 1.84−1.74 (m, 2H), 1.31−1.26 (m, 12H). ^{13}C NMR (75 MHz, $CDCl_3$, Me_4Si, 25 °C) δ_C ppm: 190.8, 165.1, 139.2, 132.0, 129.8, 114.7, 114.1, 68.4, 33.8, 29.5, 29.4, 29.3, 29.1, 28.9, 25.9. m/z (ESMS): 297 ($[M + Na]^+$, 100%). m/z (HRMS): found, 297.1828; calcd mass for $C_{18}H_{26}O_2Na$, 297.1831.

Compound ***2***. 4-Fluorobenzylamine (1.23 g, 9.84 mmol) was added to a solution of **1** (2.70 g, 9.85 mmol) in PhMe (15 mL) and stirred under reflux in a N_2(g) atmosphere for 20 h. The reaction mixture was allowed to cool to room temperature and the solvent was removed in

vacuo to afford a white precipitate. A suspension of $NaBH_4$ (0.72 g, 19.74 mmol) in MeOH (15 mL) was added dropwise to the white precipitate and the resultant solution was heated under reflux in a N_2(g) atmosphere for 16 h. The reaction mixture was partitioned in 2 M HCl (20 mL) and DCM (20 mL). The aqueous layer was extracted with DCM (2 × 25 mL), dried ($MgSO_4$), filtered and solvent removed in vacuo. The resultant crude oil was purified by flash column chromatography (eluent: hexane) to yield a colorless oil (3.21 g, 85%). ^{1}H NMR (300 MHz, $CDCl_3$, Me_4Si, 25 °C) δ_H ppm: 7.30−7.25 (m, 2H), 7.21 (d, 2H, J = 8.64 Hz), 6.99 (t, 2H, J = 8.64 Hz), 6.84 (d, 2H, J = 8.64 Hz), 5.86−5.73 (m, 1H), 5.03−4.90 (m, 2H), 3.92 (t, 2H, J = 6.50 Hz), 3.73 (s, 2H), 3.70 (s, 2H), 2.06−1.99 (m, 2H), 1.80−1.73 (m, 2H), 1.43−1.29 (m, 12H). ^{13}C NMR (75 MHz, $CDCl_3$, Me_4Si, 25 °C) δ_C ppm: 163.1, 160.7, 158.3, 139.2, 136.1, 129.7, 129.3, 115.2, 114.4, 114.1, 68.0, 52.6, 52.3, 33.8, 29.5, 29.4, 29.3, 29.1, 28.9, 26.1. m/z (ESMS): 384 ([M + Na]$^+$, 100%). m/z (HRMS): found, 384.2696; calcd mass for $C_{25}H_{35}NOFNa$, 384.2703.

Compound ***3***. A solution of Boc_2O (1.33 g, 5.94 mmol) in THF (10 mL) was added dropwise at 0 °C under a N_2(g) atmosphere to a solution of compound **2** (1.90 g, 4.95 mmol), NEt_3 (1.00 g, 9.90 mmol), and 4-DMAP (catalytic amount) in THF (15 mL) and further stirred for 16 h at room temperature under a N_2(g) atmosphere. The reaction mixture was quenched with H_2O (20 mL) and the aqueous layer was extracted with EtOAc (2 × 20 mL), dried ($MgSO_4$), filtered and concentrated in vacuo. The resultant crude oil was purified by flash column chromatography (gradient elution; from 0 to 10% EtOAc in hexane, increase in increments of 5% per 100 mL of eluent) and solvent was removed in vacuo to yield a colorless oil (1.70 g, 71%). ^{1}H NMR (300 MHz, $CDCl_3$, Me_4Si, 25 °C) δ_H ppm: 7.15 (bs, 4H), 7.02 (t, 2H, J = 9.71 Hz), 6.87 (d, 2H, J = 9.71 Hz), 5.92−5.79 (m, 1H), 5.09−4.98 (m, 2H), 4.36−4.28 (bm, 4H), 3.98 (t, 2H, J = 6.43 Hz), 2.19−1.2.14 (m, 2H), 1.87−1.78 (m, 2H), 1.66−1.52 (m, 12H). ^{13}C NMR (75 MHz, $CDCl_3$, Me_4Si, 25 °C) δ_C ppm: 163.3, 160.8, 158.5, 155.9, 139.2, 133.9, 129.7, 128.8, 115.4, 114.5, 114.1, 80.1, 68.1, 48.5, 48.0, 33.8, 29.5, 29.4, 29.3, 29.1, 28.5, 26.1. m/z 506 ([M + Na]$^+$, 100%). m/z (HRMS): found, 506.3047; calcd mass for $C_{30}H_{42}NO_3NaF$, 506.3046.

Compound ***4***. A solution of compound **3** (3.23 g, 6.68 mmol), thioacetic acid (0.76 g, 10.00 mmol), and AIBN (catalytic amount) in PhMe (10 mL) was heated under reflux for 2 h. The reaction mixture was allowed to cool to room temperature and saturated $NaHCO_3$ (25 mL) was added to the mixture, subsequently the aqueous layer was extracted with DCM (3 × 25 mL). The combined organic layers were dried ($MgSO_4$), filtered and concentrated in vacuo. The resultant crude oil was purified by flash column chromatography (gradient elution; from 0 to 10% EtOAc in hexane, increase in increments of 5% per 100 mL of eluent) and the solvent was removed to yield a colorless oil (3.27 g, 84%). ^{1}H NMR (300 MHz, $CDCl_3$, Me_4Si, 25 °C) δ_H ppm: 7.14 (bs, 4H), 7.02 (t, 2H, J = 8.72 Hz), 6.85 (d, 2H, J = 8.72 Hz), 4.35−4.28 (bm, 4H), 3.96 (t, 2H, J = 6.44 Hz), 2.88 (t, 2H, J = 7.26 Hz), 2.34 (s, 3H), 1.82−1.77 (m, 2H), 1.65−1.60 (m, 2H), 1.51−1.45 (m, 14H). ^{13}C NMR (75 MHz, $CDCl_3$, Me_4Si, 25 °C) δ_C ppm 196.0, 163.0, 158.4, 155.9, 133.9, 129.7, 115.4, 115.2, 114.5, 80.1, 67.8, 60.4, 48.4, 30.6, 29.5, 29.4, 29.3, 29.1, 28.8, 28.5, 26.1. m/z (ESMS): 582 ([M]$^+$, 100%). m/z (HRMS): found, 582.3042; calcd mass for $C_{32}H_{46}NO_4SF$, 582.3029.

Compound ***5***. A solution of TFA (8 mL) in DCM (20 mL) was added dropwise at 0 °C under a N_2(g) atmosphere to a solution of compound **4** (2.30 g, 4.11 mmol) in DCM (30 mL). The resultant reaction mixture was further stirred at room temperature for 6 h, followed by the removal of solvent in vacuo. The resultant crude oil was purified by flash column chromatography (gradient elution; from 0 to 75% EtOAc in hexane, increase in increments of 25% per 100 mL of eluent) and the solvent was removed to yield a colorless oil (1.44 g, 80%). ^{1}H NMR (300 MHz, $CDCl_3$, Me_4Si, 25 °C) δ_H ppm: 7.30−7.25 (m, 2H), 7.21 (d, 2H, J = 8.64 Hz), 6.99 (t, 2H, J = 8.64 Hz), 6.84 (d, 2H, J = 8.64 Hz), 3.92 (t, 2H, J = 6.50 Hz), 3.73 (s, 2H), 3.70 (s, 2H), 2.88 (t, 2H, J = 7.26 Hz), 2.34 (s, 3H), 2.06−1.99 (m, 2H), 1.80−1.73 (m, 2H), 1.43−1.29 (m, 14H). ^{13}C NMR (75 MHz, $CDCl_3$, Me_4Si, 25 °C) δ_C ppm: 196.0, 163.1, 160.7, 158.2, 135.8, 131.9, 129.8, 129.3, 115.2, 114.4, 67.8, 52.4, 52.1, 30.6, 29.5, 29.4, 29.3, 29.2, 29.0, 28.5, 25.6, 21.0. m/z (ESMS): 460 ([M + Na]$^+$, 100%). m/z (HRMS): found, 460.2679; calcd mass for $C_{27}H_{39}NO_2SF$, 460.2686.

Compound ***6***. A solution of compound **5** (0.96 g, 2.19 mmol) in 0.1 M HCl methanolic solution (100 mL) was heated under reflux for 4 h under a N_2 atmosphere. The resultant reaction mixture was concentrated in vacuo. The resultant crude solid was dissolved in a minimum amount of DCM and adsorbed onto silica followed by purification via flash column chromatography (gradient elution; 0 to 20% EtOAc in hexane, increase in increments of 10% after 100 mL of eluent). The solvent was removed and the resultant solid was recrystallized from EtOH to yield white solid (0.71 g, 71%). ^{1}H NMR (300 MHz, $CDCl_3$, Me_4Si, 25 °C) δ_H ppm: 7.46−7.42 (m, 2H), 7.34 (d, 2H, J = 8.60 Hz), 7.02 (t, 2H, J = 8.60 Hz), 6.84 (d, 2H, J = 8.60 Hz), 3.83 (t, 2H, J = 6.40 Hz), 3.78 (s, 2H), 3.73 (s, 2H), 2.52 (q, 2H, J = 7.10 Hz), 1.72−1.67 (m, 2H), 1.58−1.53 (m, 2H), 1.31−1.26 (m, 15H). ^{13}C NMR (75 MHz, $CDCl_3$, Me_4Si, 25 °C) δ_C ppm: 164.4, 160.1, 132.1, 131.7, 131.6, 125.6, 121.2, 116.4, 115.1, 68.1, 49.3, 48.7, 34.1, 29.6, 29.5, 29.2, 28.3, 26.1, 24.8. m/z (ESMS): 460 ([M − Cl]$^+$, 100%). m/z (HRMS): found, 418.2570; calcd mass for $C_{25}H_{37}NO_2SF$, 418.2580.

DBA-SH. To a solution of compound **6** (0.59 g, 1.30 mmol) in DCM (20 mL) was added hexafluorophosphoric acid (60% in water, 0.20 mL, 1.45 mmol) dropwise at 0 °C under a N_2 atmosphere. The resultant reaction mixture was stirred for a further 10 min at room temperature. After 10 min, H_2O (20 mL) was added and the aqueous layer was extracted with DCM (2 × 20 mL). The combined organic layers were dried ($MgSO_4$), filtered and the solvent removed in vacuo. The resultant crude solid was purified by flash column chromatography (gradient elution; from 0 to 10% MeOH in DCM, increase in increments of 2.5% per 100 mL of eluent) and the solvent was removed to yield a white solid (0.68 g, 91%). (^{1}H NMR (300 MHz, $CDCl_3$, Me_4Si, 25 °C) δ_H ppm: ^{1}H NMR (300 MHz, $CDCl_3$, Me_4Si, 25 °C) δ_H ppm: 8.53 (brs, 2H), 7.41−7.37 (m, 2H), 7.28 (d, 2H, J = 8.55 Hz), 7.03 (t, 2H, J = 8.55 Hz), 6.83 (d, 2H, J = 8.55 Hz), 3.89−3.84 (m, 4H), 3.80 (t, 2H, J = 6.55 Hz), 2.50 (q, 2H, J = 7.30 Hz), 1.72−1.67 (m, 2H), 1.58−1.53 (m, 2H), 1.31−1.26 (m, 15H). ^{13}C NMR (75 MHz, $CDCl_3$, Me_4Si, 25 °C) δ_C ppm: 164.6, 160.2, 132.2, 131.6, 131.6, 125.7, 121.1, 116.3, 115.1, 68.1, 49.4, 48.8, 34.0, 29.5, 29.4, 29.1, 28.4, 26.0, 24.7. m/z (ESMS): 418 ([M − PF_6]$^+$, 100%). m/z (HRMS): found, 418.2589; calcd mass for $C_{25}H_{37}NO_2SF$, 418.2580.

Synthesis of [G1]-DB24C8 and [G2]-DB24C8. *Compound* ***8***. A solution of NaOH (0.22 g, 5.50 mmol) in H_2O (1 mL) was added to a solution of compound **7** (1.44 g, 2.77 mmol) in EtOH (10 mL) and the resultant reaction mixture was heated under reflux for 16 h. The reaction mixture was allowed to cool to room temperature and acidified with 0.1 M HCl, whereupon a white precipitate was formed that was collected by suction filtration (1.07 g, 80%). ^{1}H NMR (300 MHz, $CDCl_3$, Me_4Si, 25 °C) δ_H ppm: 7.72 (dd, 2H, J = 1.98, J = 8.86 Hz), 7.57 (d, 1H, J = 1.98 Hz), 6.87−6.91 (m, 5H), 4.16−4.23 (m, 8H), 3.93−3.99 (m, 8H), 3.86−3.87 (m, 8H). ^{13}C NMR (75 MHz, $CDCl_3$, Me_4Si, 25 °C) δ_C ppm: 170.9, 165.4, 152.1, 148.9, 148.3, 125.6, 124.8, 121.8, 121.4, 114.6, 114.0, 112.0, 71.5, 71.4, 71.3, 70.0, 69.8, 69.6, 69.5, 69.4. m/z (ESMS): 491 ([M − H]$^+$, 100%). m/z (HRMS): found, 491.1913; calcd mass for $C_{25}H_{31}O_{10}$, 491.1917.

[G1]-DB24C8. 1-(3-(Dimethylamino)propyl)-3-ethyl-carbodiimide hydrochloride (DCC) (1.11 g, 1.14 mmol) was added to an ice bath cooled solution of compound **8** (0.50 g, 2.44 mmol), [G1][21] (0.48 g, 1.12 mmol) and catalytical amount of 4-DMAP in dry DCM (70 mL) under a N_2(g) atmosphere over 5 min. The solution was further stirred at room temperature under a $N_{2(g)}$ atmosphere for 20 h and the solvent was removed in vacuo. The resultant crude solid was dissolved in a minimum amount of DCM and absorbed onto silica followed by purification via flash column chromatography (graded elution: 0 to 10% EtOAc in hexane, increments of 5% per 150 mL of eluent used). The solvent was removed in vacuo to yield a white solid (0.50 g, 54%). ^{1}H NMR (300 MHz, $CDCl_3$, Me_4Si, 25 °C) δ_H ppm: 7.66 (d, 1H, J = 9.00 Hz), 7.55 (s, 1H), 7.24−7.41 (m, 8H), 6.87−6.91 (m, 5H), 6.66 (s, 2H), 6.58 (s, 1H), 5.25 (s, 2H), 4.95 (s, 4H), 4.05−4.18 (m, 8H), 3.92−3.97 (m, 8H), 1.31 (s, 18H). ^{13}C NMR (75 MHz, $CDCl_3$,

Me_4Si, 25 °C) δ_C ppm: 190.0, 166.1, 160.2, 153.1, 151.1, 148.9, 148.3, 138.5, 133.7, 127.6, 125.6, 124.1, 122.8, 121.4, 114.5, 114.1, 112.0, 106.9, 101.5, 71.5, 71.4, 71.3, 70.0, 69.8, 69.6, 69.4, 66.4, 31.3. *m/z* (ESMS): 929 ($[M]^+$, 100%). *m/z* (HRMS): found, 929.4502; calcd mass for $C_{54}H_{66}O_{12}$, 929.4452.

[G2]-DB24C8. According to the synthetic procedure described for [G1]-DB24C8, compound **8** (0.25 g, 0.51 mmol), [G2][21] (0.54 g, 0.55 mmol), DCC (0.05 g, 0.66 mmol), and DMAP (catalytic amount) were reacted in DCM (35 mL) and purified by flash column chromatography (graded elution: 0 to 10% EtOAc in hexane, increments of 5% per 150 mL of eluent used) to afford white crystals (0.35 g, 24%). ^{1}H NMR (300 MHz, $CDCl_3$, Me_4Si, 25 °C) δ_H ppm: 7.66 (dd, 1H, *J* = 1.90, 9.00 Hz), 7.53 (d, 1H *J* = 1.90 Hz), 7.38 (d, 8H, *J* = 8.45 Hz), 7.34 (d, 8H, *J* = 8.50 Hz), 6.87−6.91 (m, 5H), 6.66 (s, 4H), 6.58 (s, 2H), 5.25 (s, 2H), 4.95 (s, 8H), 4.05−4.18 (m, 8H), 3.92−3.97 (m, 8H), 3.81 (d, 8H, *J* = 9.00 Hz), 1.31 (s, 36H). ^{13}C NMR (75 MHz, $CDCl_3$, Me_4Si, 25 °C) δ_C ppm: 190.0, 166.1, 160.2, 153.1, 151.1, 148.9, 148.3, 138.5, 133.7, 127.6, 125.6, 124.1, 122.8, 121.4, 114.5, 114.1, 112.0, 106.9, 101.5, 71.5, 71.4, 71.3, 70.0, 69.8, 69.6, 69.4, 66.4, 31.3. *m/z* (ESMS), 1465 ($[M + Na]^+$, 100%); *m/z* (HRMS): found, 1465.7309; calcd mass for $C_{90}H_{106}O_{16}Na$, 1465.7379.

Compound Characterization. *NMR.* ^{1}H nuclear magnetic resonance (NMR) spectra were recorded on a Bruker AVIII300 (300.13 MHz) spectrometer. ^{13}C NMR spectra were recorded on a Bruker AVIII 400 (75.5 MHz) using Pendent pulse sequences. All chemical shifts are quoted in ppm to higher frequency from Me_4Si using either deuterated chloroform ($CDCl_3$) or methanol (CD_3OD) as the lock and the residual solvent as the internal standard. The coupling constants are expressed in hertz (Hz) with multiplicities abbreviated as follows: s = singlet, d = doublet, dd = double doublet, t = triplet, q = quartet, and m = multiplet.

Mass spectrometry (MS). Electron impact mass spectroscopy (EIMS) was performed on a VG Prospec. Low- and high-resolution electrospray mass spectrometry was performed on a Micromass time-of-flight (TOF) instrument using methanol as the mobile phase.

SAM Preparation and Characterization. *Preparation of SAMs.* Polycrystalline gold substrates were purchased from George Albert PVD, Germany, and consisted of either a 50 nm gold layer deposited onto glass covered with a thin layer (5 nm) of chromium as the adhesion layer (used for contact angle analysis) or 100 nm thickness on 100−4 in.-silicon wafer, precoated with titanium as the adhesion layer (for ellipsometry and XPS analysis). The Au substrates were rinsed with HPLC EtOH and Ultra High Pure (UHP) H_2O (resistivity = 18 MΩ cm), dried with a stream N_2(g), exposed to UV light for 1 h, and submerged in HPLC EtOH until they were used, which was no longer than 30 min. Prior to being immersed in the DB24C8⊃DBA-SH, [G1]-DB24C8⊃DBA-SH and [G2]-DB24C8⊃DBA-SH solutions, the substrates were rinsed thoroughly with copius amounts of HPLC EtOH followed by rinsing with HPLC MeCN. The complexation between the dialkylammonium anion (DBA-SH) and the DB24C8 derivatives (DB24C8, [G1]-DB24C8 and [G2]-DB24C8) was carried out in HPLC MeCN (1 mM). To a solution of DBA-SH (0.01 mmol) in HPLC MeCN (1 mL) were added the DB24C8 derivatives (0.02 mmol), and the resultant solution was stirred for 10 min. The Au substrates were immersed in the solutions of the supramolecular complexes for 24 h, followed by thorough rinsing with HPLC MeCN and subsequently submerged into a mixed HPLC MeCN solution of 2 mM NEt_3 and 1 mM ClPrSH for 30 min. The substrates were removed from the solution and rinsed with copious amounts of HPLC MeCN and dried with a stream N_2(g).

Contact Angle Measurements. Dynamic contact angles were determined using a home-built contact angle apparatus, equipped with a charged coupled device (CCD) KP-M1E/K camera (Hitachi) that was attached to a personal computer for video capture. FTA Video Analysis software v1.96 (First Ten Angstroms) was used for the analysis of the contact angle of a droplet of UHQ H_2O at the three-phase intersection. The dynamic contact angles were recorded as a microsyringe was used to quasi-statically add liquid to or remove liquid from the drop. The drop was shown as a live video image on the PC screen and digitally recorded for future analysis. The acquisition rate was 4 frames per second. The contact angles were determined from an average of five different measurements made for each type of SAM. The errors reported for the contact angle measurements are standard errors.

Ellipsometry Measurements. The thickness of the deposited monolayers was determined by spectroscopic ellipsometry. A Jobin-Yvon UVISEL ellipsometer with a xenon light source was used for the measurements. The angle of incidence was fixed at 70°. A wavelength range of 280−800 nm was used. The DeltaPsi software was employed to determine the thickness values and the calculations were based on a three-phase ambient/SAM/Au model, in which the SAM was assumed to be isotropic and assigned a refractive index of 1.50. The thickness reported is the average of six measurements taken on each SAM. The errors reported for the ellipsometry measurements are standard errors.

X-ray Photoelectron Spectroscopy (XPS). XPS spectra were obtained using an Escalab 250 system (Thermo VG Scientific) operating with Avantage v1.85 software under a pressure of $\sim 5 \times 10^{-9}$ mbar. An Al Kα X-ray source was used that provided a monochromatic X-ray beam with incident energy of 1486.68 eV. A circular spot size of $\sim$0.2 mm^2 was employed. The samples were attached onto a stainless steel holder using double-sided carbon sticky tape (Shintron tape). Low resolution survey spectra were obtained using a pass energy of 150 eV over a binding energy range of 210 to 1200 eV obtained using 1 eV increments. The spectra recorded were an average of 3 scans. The high resolution spectra were obtained using a pass energy of 20 and 0.1 eV increments over a binding energy range of 20−30 eV, centered at the binding energy characteristic of the functional group. A dwell time of 20 ms was employed between each binding energy increment. Sensitivity factors used in this study were: S (2p), 2.08; Au (4f 7/2), 9.58; Au (4f 5/2), 7.54, C (1s), 1, F (1s) 5.1, O (1s) 2.6.

Electrochemistry. Electrochemical studies were performed with a Gamry 600 potentiostat and data acquisition software (Gamry electrochemistry software version 5.61a) in a three-electrode Teflon cell consisting of a saturated calomel reference electrode (SCE), Pt wire counter electrode and the gold modified with different SAMs as the working electrode. Linear sweep voltammetry was performed to investigate the thiol reductive desorption. A starting potential of +0.3 V and an end potential of +1.3 V at a scan rate 100 mV s^{-1} was used. The electrolyte was a 0.5 M KOH solution prepared fresh each day. The voltammograms were performed in triplicate with a new working electrodes modified with the relevant SAM for each replicate. The geometric area was controlled by use of a 4 mm diameter O-ring.

■ ASSOCIATED CONTENT

Ⓢ Supporting Information

Additional experimental details and figures. This material is available free of charge via the Internet at http://pubs.acs.org.

■ AUTHOR INFORMATION

Corresponding Author

*E-mail: p.m.mendes@bham.ac.uk. Tel: +(121) 414-5343.

Notes

The authors declare no competing financial interest.

■ ACKNOWLEDGMENTS

The authors acknowledge financial support of this work by the Leverhulme Trust (F/00094/AW, F/00094/BD and ECF/2013-603), Royal Society (2009/R3), Wellcome Trust (WT091285MA), EPSRC (EP/K027263/1), the European Commission under the FP7-NMP project Hysens (263091), the Research Grants Council of Hong Kong (201412), and the University Grants Committee of Hong Kong SAR (AoE/P-03/08). Also, we acknowledge the University of Leeds EPSRC Nanoscience and Nanotechnology Facility (LENNF) for access to the XPS. This research was in part supported through Birmingham Science City: Innovative Uses for Advanced

Materials in the Modern World (West Midlands Centre for Advanced Materials Project 2), supported by Advantage West Midlands (AWM) and part funded by the European Regional Development Fund (ERDF). This work was also supported by the National Basic Research Program (2011CB808604) and the National Natural Science Foundation of China (21273102). We are grateful to the High Performance Computing Centre of Nanjing University for providing the IBM Blade cluster system.

REFERENCES

(1) Mendes, P. M. Stimuli-Responsive Surfaces for Bio-Applications. *Chem. Soc. Rev.* **2008**, *37*, 2512−2529.
(2) Demidov, V. V. Nanobiosensors and Molecular Diagnostics: A Promising Partnership. *Expert Rev. Mol. Diagn.* **2004**, *4*, 267−268.
(3) Niemeyer, C. M.; Mirkin, C. A.. *Nanobiotechnology*; Wiley-VCH Verlag GmbH & Co. KGaA: Weinheim, Germany, 2004.
(4) Mendes, P. M. Cellular Nanotechnology: Making Biological Interfaces Smarter. *Chem. Soc. Rev.* **2013**, *42*, 9207−9218.
(5) Smits, E. C. P.; Mathijssen, S. G. J.; van Hal, P. A.; Setayesh, S.; Geuns, T. C. T.; Mutsaers, K.; Cantatore, E.; Wondergem, H. J.; Werzer, O.; Resel, R.; Kemerink, M.; Kirchmeyer, S.; Muzafarov, A. M.; Ponomarenko, S. A.; de Boer, B.; Blom, P. W. M.; de Leeuw, D. M. Bottom-Up Organic Integrated Circuits. *Nature* **2008**, *455*, 956−959.
(6) Sagiv, J. Organized Monolayers by Adsorption 0.1. Formation and Structure of Oleophobic Mixed Monolayers on Solid-Surfaces. *J. Am. Chem. Soc.* **1980**, *102*, 92−98.
(7) Nuzzo, R. G.; Allara, D. L. Adsorption of Bifunctional Organic Disulfides on Gold Surfaces. *J. Am. Chem. Soc.* **1983**, *105*, 4481−4483.
(8) Lahiri, J.; Isaacs, L.; Tien, J.; Whitesides, G. M. A Strategy for the Generation of Surfaces Presenting Ligands for Studies of Binding Based on an Active Ester as a Common Reactive Intermediate: A Surface Plasmon Resonance Study. *Anal. Chem.* **1999**, *71*, 777−790.
(9) Mendes, P. M.; Yeung, C. L.; Preece, J. A. Bio-Nanopatterning of Surfaces. *Nanoscale Res. Lett.* **2007**, *2*, 373−384.
(10) Mrksich, M. Dynamic Substrates for Cell Biology. *MRS Bull.* **2005**, *30*, 180−184.
(11) Mrksich, M. What Can Surface Chemistry Do for Cell Biology? *Curr. Opin. Chem. Biol.* **2002**, *6*, 794−797.
(12) Pranzetti, A.; Mieszkin, S.; Iqbal, P.; Rawson, F. J.; Callow, M. E.; Callow, J. A.; Koelsch, P.; Preece, J. A.; Mendes, P. M. An Electrically Reversible Switchable Surface to Control and Study Early Bacterial Adhesion Dynamics in Real-Time. *Adv. Mater.* **2013**, *25*, 2181−2185.
(13) Leung, K. C.-F.; Xuan, S.; Lo, C.-M. Reversible Switching between Hydrophilic and Hydrophobic Superparamagnetic Iron Oxide Microspheres via One-Step Supramolecular Dynamic Dendronization: Exploration of Dynamic Wettability. *ACS Appl. Mater. Interfaces* **2009**, *1*, 2005−2012.
(14) Stephenson-Brown, A.; Wang, H. C.; Iqbal, P.; Preece, J. A.; Long, Y. T.; Fossey, J. S.; James, T. D.; Mendes, P. M. Glucose Selective Surface Plasmon Resonance-Based Bis-Boronic Acid Sensor. *Analyst* **2013**, *138*, 7140−7145.
(15) Laibinis, P. E.; Fox, M. A.; Folkers, J. P.; Whitesides, G. M. Comparisons of Self-Assembled Monolayers on Silver and Gold - Mixed Monolayers Derived from HS(CH2)21X and HS(CH2)10Y (X, Y = CH3, CH2OH) Have Similar Properties. *Langmuir* **1991**, *7*, 3167−3173.
(16) Tamada, K.; Hara, M.; Sasabe, H.; Knoll, W. Surface Phase Behavior of N-Alkanethiol Self-Assembled Monolayers Adsorbed on Au(111): An Atomic Force Microscope Study. *Langmuir* **1997**, *13*, 1558−1566.
(17) Hobara, D.; Ota, M.; Imabayashi, S.; Niki, K.; Kakiuchi, T. Phase Separation of Binary Self-Assembled Thiol Monolayers Composed of 1-Hexadecanethiol and 3-Mercaptopropionic Acid on Au(111) Studied by Scanning Tunneling Microscopy and Cyclic Voltammetry. *J. Electroanal. Chem.* **1998**, *444*, 113−119.
(18) Sawaguchi, T.; Sato, Y.; Mizutani, F. In Situ STM Imaging of Individual Molecules in Two-Component Self-Assembled Monolayers of 3-Mercaptopropionic Acid and 1-Decanethiol on Au(111). *J. Electroanal. Chem.* **2001**, *496*, 50−60.
(19) Tomalia, D. A.; Mardel, K.; Henderson, S. A.; Holan, G.; Esfand, R.: Dendrimers — An Enabling Synthetic Science to Controlled Organic Nanostructures In *Handbook of Nanoscience, Engineering, and Technology*; CRC Press: Boca Raton, FL, 2003; pp 20−21−20−34.
(20) Ashton, P. R.; Campbell, P. J.; Chrystal, E. J. T.; Glink, P. T.; Menzer, S.; Philp, D.; Spencer, N.; Stoddart, J. F.; Tasker, P. A.; Williams, D. J. Dialkylammonium Ion Crown-Ether Complexes - The Forerunners of a New Family of Interlocked Molecules. *Angew. Chem., Int. Ed.* **1995**, *34*, 1865−1869.
(21) Leung, K. C. F.; Mendes, P. M.; Magonov, S. N.; Northrop, B. H.; Kim, S.; Patel, K.; Flood, A. H.; Tseng, H. R.; Stoddart, J. F. Supramolecular Self-Assembly of Dendronized Polymers: Reversible Control of the Polymer Architectures Through Acid-Base Reactions. *J. Am. Chem. Soc.* **2006**, *128*, 10707−10715.
(22) Chak, C. P.; Xuan, S. H.; Mendes, P. M.; Yu, J. C.; Cheng, C. H. K.; Leung, K. C. F. Discrete Functional Gold Nanoparticles: Hydrogen Bond-Assisted Synthesis, Magnetic Purification, Supramolecular Dimer and Trimer Formation. *ACS Nano* **2009**, *3*, 2129−2138.
(23) Chak, C. P.; Chau, L. H.; Wu, S. Y.; Ho, H. P.; Li, W. J.; Mendes, P. M.; Leung, K. C. F. Simultaneous Purification and Surface Plasmon Resonance Characterization of Mechanoresponsive, Discretely Functionalized Gold Nanoparticles. *J. Mater. Chem.* **2011**, *21*, 8317−8323.
(24) Ho, W. K. W.; Lee, S. F.; Wong, C. H.; Zhu, X. M.; Kwan, C. S.; Chak, C. P.; Mendes, P. M.; Cheng, C. H. K.; Leung, K. C. F. Type III-B Rotaxane Dendrimers. *Chem. Commun.* **2013**, *49*, 10781−10783.
(25) Schonherr, H.; Ringsdorf, H. Self-Assembled Monolayers of Symmetrical and Mixed Alkyl Fluoroalkyl Disulfides on Gold 0.1. Synthesis of Disulfides and Investigation of Monolayer Properties. *Langmuir* **1996**, *12*, 3891−3897.
(26) James, M.; Darwish, T. A.; Ciampi, S.; Sylvester, S. O.; Zhang, Z. M.; Ng, A.; Gooding, J. J.; Hanley, T. L. Nanoscale Condensation of Water on Self-Assembled Monolayers. *Soft Matter* **2011**, *7*, 5309−5318.
(27) Porter, M. D.; Bright, T. B.; Allara, D. L.; Chidsey, C. E. D. Spontaneously Organized Molecular Assemblies 0.4. Structural Characterization of Normal-Alkyl Thiol Monolayers on Gold by Optical Ellipsometry, Infrared-Spectroscopy, and Electrochemistry. *J. Am. Chem. Soc.* **1987**, *109*, 3559−3568.
(28) Cassie, A. B. D. Contact Angles. *Discuss. Faraday Soc.* **1948**, *3*, 11−16.
(29) Yeung, C. L.; Charlesworth, S.; Iqbal, P.; Bowen, J.; Preece, J. A.; Mendes, P. M. Different Formation Kinetics and Photoisomerization Behavior of Self-Assembled Monolayers of Thiols and Dithiolanes Bearing Azobenzene Moieties. *Phys. Chem. Chem. Phys.* **2013**, *15*, 11014−11024.
(30) Traub, M. C.; Biteen, J. S.; Michalak, D. J.; Webb, L. J.; Brunschwig, B. S.; Lewis, N. S. High-Resolution X-Ray Photoelectron Spectroscopy of Chlorine-Terminated GaAs(111)A Surfaces. *J. Phys. Chem. B* **2006**, *110*, 15641−15644.
(31) Moulder, J. F.; Stickle, W. F.; Sobol, P. E.; Bomben, K. D.: *Handbook of X-ray Photoelectron Spectroscopy*; Perkin-Elmer Corp: Eden Prairie, MN, 1992.
(32) Luo, M.; Frechette, J. Electrochemical Stability of Low-Density Carboxylic Acid Terminated Monolayers. *J. Phys. Chem. C* **2010**, *114*, 20167−20172.
(33) Laredo, T.; Leitch, J.; Chen, M.; Burgess, I. J.; Dutcher, J. R.; Lipkowski, J. Measurement of the Charge Number Per Adsorbed Molecule and Packing Densities of Self-Assembled Long-Chain Monolayers of Thiols. *Langmuir* **2007**, *23*, 6205−6211.
(34) Świetlow, A.; Skoog, M.; Johansson, G. Double-Layer Capacitance Measurements of Self-Assembled Layers on Gold Electrodes. *Electroanalysis* **1992**, *4*, 921−928.

(35) Ionita, P.; Volkov, A.; Jeschke, G.; Chechik, V. Lateral Diffusion of Thiol Ligands on The Surface of Au Nanoparticles: An Electron Paramagnetic Resonance Study. *Anal. Chem.* **2008**, *80*, 95−106.
(36) Lussem, B.; Muller-Meskamp, L.; Karthauser, S.; Waser, R.; Homberger, M.; Simon, U. STM Study of Mixed Alkanethiol/Biphenylthiol Self-Assembled Monolayers on Au(111). *Langmuir* **2006**, *22*, 3021−3027.
(37) Schonherr, H.; Ringsdorf, H.; Jaschke, M.; Butt, H. J.; Bamberg, E.; Allinson, H.; Evans, S. D. Self-Assembled Monolayers of Symmetrical and Mixed Alkyl Fluoroalkyl Disulfides on Gold 0.2. Investigation of Thermal Stability and Phase Separation. *Langmuir* **1996**, *12*, 3898−3904.
(38) Imabayashi, S.; Hobara, D.; Kakiuchi, T. Voltammetric Detection of the Surface Diffusion of Adsorbed Thiolate Molecules in Artificially Phase-Separated Binary Self-Assembled Monolayers on A Au(111) Surface. *Langmuir* **2001**, *17*, 2560−2563.
(39) Peng, D. K.; Lahann, J. Chemical, Electrochemical, and Structural Stability of Low-Density Self-Assembled Monolayers. *Langmuir* **2007**, *23*, 10184−10189.